SQUID-based measurement of biomagnetic fields

M. P. Janawadkar, T. S. Radhakrishnan, K. Gireesan, C. Parasakthi, S. Sengottuvel, Rajesh Patel, C. S. Sundar and Baldev Raj*

This article reports the establishment of the first facility in India for the superconducting quantum interference device (SQUID) based measurement of extremely weak magnetic fields such as those associated with the physiological activities of human heart (~50 pico-Tesla) and human brain (100 femto-Tesla to 2 pico-Tesla). The facility comprises a magnetically shielded room capable of attenuating ambient magnetic noise by 60 dB at 1 Hz, connected by waveguides to a RF shielded room capable of attenuating RF noise by 100 dB. Magnetically shielded room houses a fibre glass reinforced plastic cryostat with four SQUID channels and the RF shielded room houses the data acquisition system. The overall system noise, measured in each channel, is under 12 fT/√Hz. Several biomagnetic fields (magnetocardiogram, α-rhythm of brain and auditory evoked response) have been successfully measured in this facility with a high signal-to-noise ratio.

Keywords: Biomagnetism, magnetoencephalography, magnetocardiography, superconducting quantum interference device.

CELLULAR transduction of signals as well as physiological control of organs and organ systems is often associated with the flow of tiny electric currents in the system of interest. These physiological processes produce a distribution of electric potential on the exterior surface of the skin and an accompanying magnetic field. The electric potential and the magnetic field constitute the quantitatively measurable attributes correlating with the underlying physiological process and hence their measurement helps in the analysis of normal functionality and also in the recognition of certain types of physiological dysfunctions. The electric potential distribution on the anterior thoracic surface is measured in electrocardiography (ECG) in order to probe the physiological activity of the heart, while that on the surface of the scalp is measured in electroencephalography (EEG) to probe the physiological activities of the human brain. The measurement of corresponding magnetic fields, which are typically about 100 femto-Tesla to 100 pico-Tesla, is a challenging task as these magnetic fields are more than a million times weaker than the earth's magnetic field of 40 micro-Tesla, whereas the ambient magnetic noise due to power-line and other sources is orders of magnitude higher (often 10 nano-Tesla to 100 nano-Tesla). There are also no sensors of magnetic field, except the superconducting quantum interference devices (SQUID), which have adequate sensitivity to measure and characterize such extremely weak magnetic fields. The measurement of biomagnetic fields, therefore, became possible only after the development of SQUID sensors[1]. Introduction of high quality thin film DC SQUID sensors in more recent times has led to a revolution in biomagnetic instrumentation; the last two decades have seen the emergence of multichannel systems housing a large number of SQUID sensors to simultaneously measure the magnetic field intensity at a set of discrete points in space and thus pave way for the reconstruction of sources responsible for the measured magnetic field distribution[2,3]. Such strategies are vital to unravel the underlying electrophysiology of human heart and human brain, and are expected to widen the horizons of scientific investigations. Compared to the conventional techniques such as ECG and EEG, which measure the electric potential on the skin surface, SQUID-based measurement of the accompanying magnetic fields offers a number of distinct advantages: magnetic measurement techniques are non-contact, much less sensitive to the conductivity variation of the underlying tissues and offer superior source localization accuracies. Indeed these are among the few physical measurements, apart from functional magnetic resonance imaging (fMRI)[4] and positron emission tomography (PET)[5], which provide quantitatively measureable macroscopic correlates of the underlying activity at the cellular level. Whereas MRI provides only anatomical structural images, fMRI is capable of giving functional information by showing cortical regions of increased activity as recognized by an increased blood

The authors are in the Indira Gandhi Centre for Atomic Research, Kalpakkam 603 102, India.
*For correspondence. (e-mail: mpj@igcar.gov.in)

flow to such regions. However, it must be noted that such techniques exploiting either a blood oxygen level dependent (BOLD) signal or an increase in glucose metabolism at a selected cortical region are limited by the relatively large time constants associated with haemodynamics and, therefore, the temporal resolution of such techniques is poor, often in the range of seconds[6]. The techniques involving measurement of electric potential in EEG or the magnetic field intensity in magnetoencephalography (MEG), on the other hand, are capable of a temporal resolution in the range of milliseconds and this opens up the possibility to investigate the generation of cortical response as it builds up in real time. By its very nature, EEG requires attachment of electrodes to the skin using a conducting gel and the measured potential distribution on the skin surface is nontrivially affected by the conductivity distribution between the source and the measurement location. Since the conductivity distribution is inhomogeneous, anisotropic and often unknown (with bones presenting very poor electrical conductivity), the accuracy of source localization using the EEG data (and hence the spatial resolution of the EEG technique) tends to be rather poor[7]. Because the MEG signals are relatively less sensitive to the conductivity distribution, analysis of MEG data enables source localization accuracies in the range of 2–3 mm to be attained in practice[8]. Thus, during the last decade, the measurement of biomagnetic fields using SQUID-based multichannel systems has opened up new vistas of scientific research.

SQUID sensors based on Nb–AlO_x–Nb Josephson junctions are the most sensitive detectors of magnetic flux available today with a routinely achieved field sensitivity of under 10 fT/√Hz. This extraordinary sensitivity, not achievable using any other sensor technology, is adequate for the measurement and characterization of the temporal variation of biomagnetic fields such as those associated with the physiological activities of human heart (typically 50 pT on the chest surface), human brain (typically 2 pT on scalp) and the responses evoked from the human brain on presentation of auditory/visual/tactile stimuli (typically 100 fT on the scalp)[9]. Because the ambient magnetic noise in the frequency range of interest (0.1–1000 Hz) is often as high as several nT, it is evident that a magnetically shielded room (MSR) with a high shielding factor of 60–100 dB is an essential prerequisite for the measurement of biomagnetic fields. Such MSR has been set up at the Indira Gandhi Centre for Atomic Research (IGCAR) as part of facilities for the measurement of biomagnetic fields, building on two decades of experience in the use of these sensors in areas such as SQUID magnetometer and non-destructive evaluation of materials[10,11]. In the last four years, key facilities leading to the establishment of measurement systems for magnetocardiography (MCG) and MEG, which share a common infrastructure, have been established at IGCAR, and several biomagnetic signals, including those from human heart and brain, have been measured successfully in these facilities with a high signal-to-noise ratio. Although a system based on four SQUID channels is currently operational and is being extensively used for biomagnetic research, a multichannel MEG system is expected to be operational soon and will enable the power of the MEG technique to be fully exploited for unravelling the mysteries of perception and analysis of sensory inputs by the human brain.

Facilities for biomagnetic research

The site for the establishment of these facilities was chosen to be at least 6 m away from all existing laboratories to avoid a high level of ambient magnetic noise. A survey of ambient magnetic noise at the chosen site was carried out to assess the suitability of the site for the intended application. The initial survey (S. G. Gokarn, private commun.) was carried out using induction coils as the sensors; the results of this initial survey were confirmed in a second site-survey (Schlaepfer Urs, private commun.) employing a flux gate sensor with a sensitivity of under 20 pT/√Hz. In the latter measurement, a three-axis flux gate sensor was used to simultaneously acquire the data related to the temporal variation of the magnetic field along each of the three mutually orthogonal directions and hence infer the spectral density of ambient magnetic noise at the selected site. Sampling rate was varied between 25 samples per second for a frequency bandwidth of 10 Hz to 2500 samples per second for a frequency bandwidth of 1000 Hz. As shown in Figure 1, the measurements at the selected site revealed the spectral density of ambient magnetic noise to be generally white with an amplitude of less than 100 pT/√Hz, whereas the noise at the power line frequency (50 Hz) was about 6 nT/√Hz. The site at IGCAR, situated away from urban populations, thus proved to be an ideal site for the location of MSR; these measurements also helped in deciding the necessary level of attenuation of these external magnetic disturbances, which will be required for the measurement of biomagnetic fields. In view of the high costs involved in low-frequency magnetic shielding, it was decided to plan for a modest shielding factor of 60 dB at 1 Hz improving to 100 dB at 100 Hz. Further reduction of the effect of the residual noise inside MSR on the measured data could be realized by the use of a superconducting first-order gradiometer consisting of two superconducting loops wound in opposition and separated along the vertical direction by a small baseline of 50 mm for coupling the signal to be measured to the SQUID sensor; the distant sources of magnetic noise produce equal and opposite responses in the two loops and thereby get rejected whereas signals from a nearby source produce a nonzero response. Combination of the passive shielding and the use of gradiometric technique to discriminate against distant sources of magnetic noise was considered to be adequate for the measurement of biomagnetic fields.

Because vibrations of the MSR, SQUID sensors and cables are important sources of noise, a concerted effort was made to reduce the vibrations to as low a value as possible. To minimize vibrations to acceptable levels under 10^{-5} g (i.e. 10^{-4} m/s^2), it was decided to install MSR on 1 m deep concrete foundation block weighing about 50 tonnes, which was isolated from the rest of the floor. Figure 2 shows the levels of vibration measured on the bare ground at the site (before the beginning of construction) and on the foundation block for MSR; it also shows the effect on the vibration levels as a tractor was driven in the neighbourhood to induce ground vibrations (Anupkumar *et al.*, MS under preparation). It may be noted that the vibration levels measured on the upper surface of the foundation block were relatively unaffected by the movement of the tractor. Further, because the conventional reinforcement of concrete uses mild steel, which is ferromagnetic and is likely to result in concentration and focusing of the magnetic flux lines in the region of interest depending upon the orientation of the mild steel rods, non-magnetic stainless steel as reinforcement in concrete (SS-RCC) was used; incidentally, the use of stainless steel also obviates the problem of unpredictable remnant magnetization of these mild steel rods due to transient magnetic disturbances as it is difficult to have provisions to fully demagnetize these structures embedded within concrete on a periodic basis. As stainless steel grade 304 has a tendency to transform and produce, when subjected to stresses, small volume fractions of martensitic phases which are magnetic[12], rods of stainless steel grade 316 were used. As no prior experience existed in India on the use of SS316 rods as reinforcement in concrete, pull-out tests were carried out in standard geometries employing M30 grade concrete to experimentally evaluate the bond strength between SS316 rods and concrete. Also, as ribbed rods of SS316 were not readily available in India (unlike their mild steel counterparts), SS316 rods with a round cross-section without smooth surface finish were used in these tests. A detailed description of the tests carried out and the results obtained have been given elsewhere[13]. This data was used for the detailed engineering design of the building in which the MSR was housed, as also of the foundation block which supported MSR (D. Prusty and C. S. Pillai, private commun.). This special building employing SS316 rods for reinforcing concrete was built at IGCAR, and represents, to our knowledge, the first such building to have been constructed in India. The effect of using stainless steel as reinforcement material has been dramatic; as shown in Figure 3, artificially created transient magnetic disturbances accompanying the movement of a heavy tractor in the neighbourhood, measuring about 240 nT in a conventional building reinforced with ferromagnetic mild steel, were found to have an amplitude below 30 nT in the special building constructed with nonmagnetic stainless steel reinforcement.

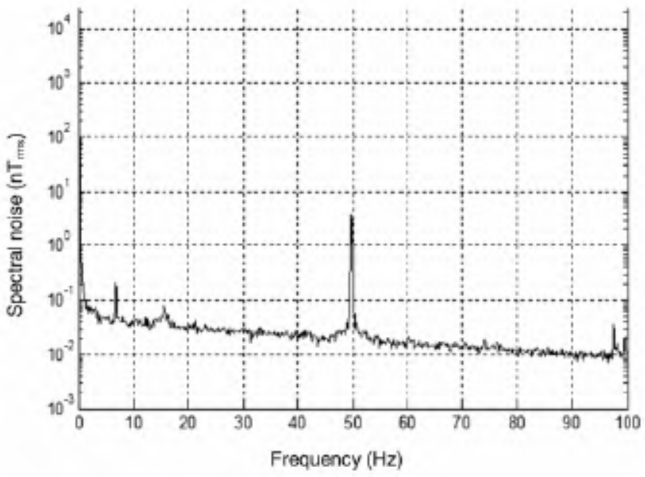

Figure 1. Site survey of the ambient magnetic noise at the site prior to the erection of MSR; the noise is under 100 pT/√Hz in the white noise regime and is 6 nT/√Hz at the power line frequency of 50 Hz. A shielding factor of 60 dB at 1 Hz (improving to 100 dB at 100 Hz) was considered to be adequate for the measurement of biomagnetic signals.

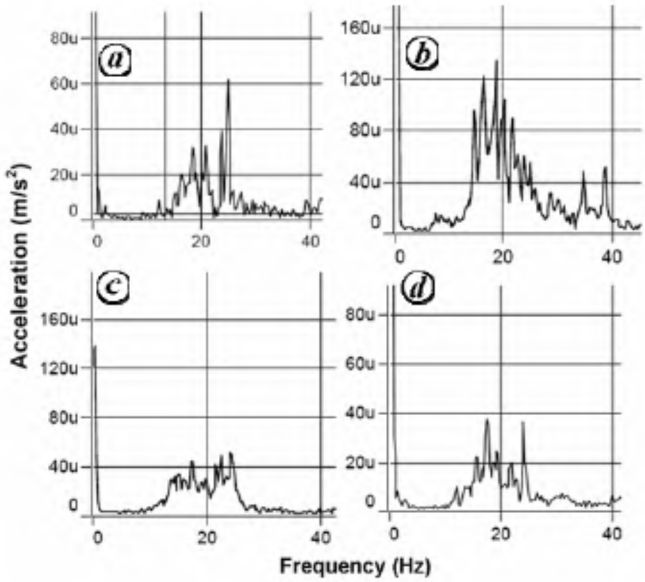

Figure 2. Vibration levels measured on ***a***, bare ground at the site and ***c***, foundation block for MSR; the panels ***b*** and ***d*** on the right show the corresponding vibration levels recorded when a heavy tractor was driven in the neighbourhood. The vibration levels on the foundation block were virtually unaltered by tractor movement in contrast to those on the bare ground. Each panel shows acceleration (μm/s^2) recorded as a function of frequency (Hz).

MSR was planned to have two layers of mu-metal (2 and 3 mm thick) to provide low-frequency magnetic shielding and two layers of high conductivity aluminium (4 and 8 mm thick) to provide high-frequency magnetic shielding with a view to realize the requisite shielding factor over the frequency range of interest. It may be noted that although a large number of MSRs have been built internationally for this purpose, none existed in India. The first MSR in India was installed and commissioned at IGCAR as part of an effort to set up facilities for SQUID-based measurement of biomagnetic fields

described here. As shown in Figure 4, the experimentally measured shielding factor provided by MSR is about 70 dB at 1 Hz improving to more than 110 dB at 100 Hz. The MSR was equipped with ports required for recovery of evaporated helium gas, for mounting a video camera to monitor the subject under investigation, for the installation of a voice communication system and for stimulus presentation to the subject as required during an experimental neuroscience investigation; in addition, a 100 mm diameter safety vent has been provided to route the helium gas safely outside the MSR, if need arises. MSR is equipped with four 100 mm diameter waveguides to route the SQUID cables into an adjoining RF shielded room (RFSR), where all the electronic instrumentation requiring the 240 V, 50 Hz mains power is located; this arrangement is to obviate any RF noise streaming inside MSR through the cables and conduits and the consequent degradation of the SQUID performance. MSR is also equipped with two large demountable panels for future use. Ten signal line feedthrough filters have been provided through which low level, low-frequency electrical signals could be routed inside MSR depending upon experimental needs. The door of MSR is 2 m in height and 1 m in width, and is pneumatically actuated. There is a built in provision to degauss the mu-metal layers of MSR whenever desired by the user. Illumination inside MSR is provided with a specially designed DC lighting system to avoid magnetic noise. MSR houses the liquid helium cryostat made of fibre reinforced plastic (FRP), the non-magnetic gantry on which the cryostat is supported and the battery powered modules comprising the preamplifier and the flux-locked-loop electronics mounted close to the top of the cryostat for processing the SQUID output signals.

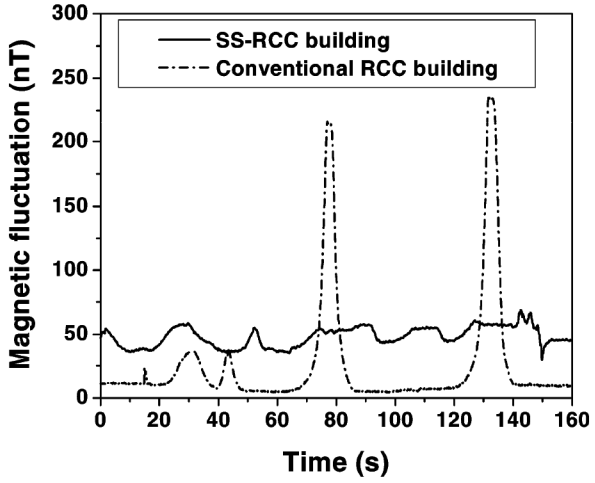

Figure 3. Plot showing magnetic fluctuation (nT) versus time. Transient magnetic disturbance recorded in conventional and SS-RCC buildings; the transient magnetic disturbances caused by a given source were found to be lower by a factor of 8 in the SS-RCC building as opposed to the conventional building employing ferromagnetic mild steel bars for reinforcement.

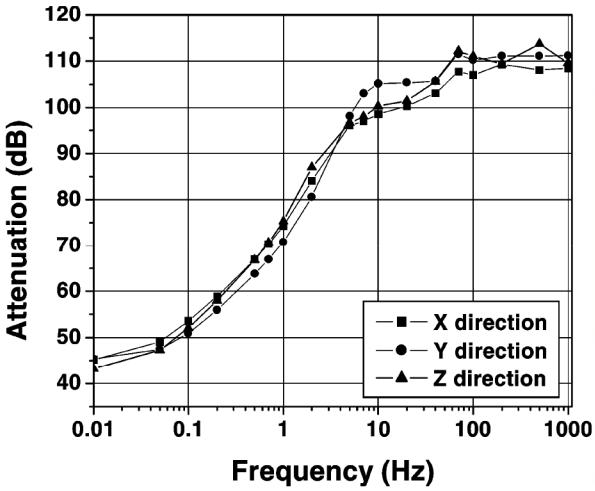

Figure 4. Plot showing attenuation (dB) versus frequency (Hz). Shielding factor of the magnetically shielded room installed at IGCAR as a function of frequency; the shielding improves from 70 dB at 1 Hz to 110 dB at 100 Hz.

A separate RFSR, connected to MSR via four 100 mm diameter waveguides, was planned to house all the electronic instrumentation requiring the mains power such as analog-to-digital conversion modules to digitize the SQUID output signal in each channel, function generators, oscilloscope and other test and measuring instrumentation required during an experiment. RFSR provides an attenuation of 100 dB at frequencies exceeding 1 MHz and is constructed using 2 mm thick aluminum sheets with high electrical conductivity. RFSR is equipped with four ports of 38 mm diameter to route optical fibres carrying the digitized signals outside RFSR to ensure noise immunity during the transfer of data to a computer located outside the shielded area. RFSR is also equipped with 10 signal line feedthrough filters through which low level, low-frequency electrical signals could be routed. Mains power for all the electronic instruments located inside the RFSR is routed via a special isolation transformer and enters the RFSR via a filter. Figure 5 shows a photograph of MSR established at IGCAR in which the liquid helium cryostat housing the SQUID sensors is located.

Figure 5. Photograph of MSR established at IGCAR for SQUID based MEG; the panel on the right shows the shielded waveguides connecting the MSR and RFSR through which SQUID cables are routed.

Generation and modelling of biomagnetic fields

The electrophysiology of excitable cells such as neurons in the human brain and myocytes in human heart is responsible for the generation of both electric and magnetic fields in space, which can be measured to obtain insights into both normal physiological response and to recognize deviations owing to any abnormal functionality. It is well known that the concentration gradient of ionic species such as Na^+, K^+, Cl^-, etc. between the intracellular and extracellular fluids gives rise to an equilibrium potential difference of about –70 mV across the cell membrane in the quiescent state in accordance with the Nernst–Goldmann equation[14]. When a cell is excited by the neurotransmitter molecules released into the synaptic cleft by the adjacent cells, permeability of the cell membrane to Na^+ ions is modified as the corresponding ion-channels open and the transmembrane potential changes from about – 70 mV to about + 20 mV due to the inflow of Na^+ ions driven by the concentration gradient; thereafter, Na^+ channels close and the transmembrane potential reverts to the quiescent value of about – 70 mV due to the opening of some voltage gated K^+ channels and the consequent outflow of K^+ ions. This transient lasts for about 2–3 millisec and is known as the action potential. Subsequently, the action of the Na–K pump powered by the ATP restores the ionic concentrations to their original values. This depolarization of the cell membrane (and its subsequent repolarization) involves transport of ions across the cell membrane, which constitutes the primary current $\mathbf{J}^p$. The primary current is accompanied by the appearance of an electric field $\mathbf{E}$ in the neighbourhood, which drives volume currents through the surrounding tissue acting as a passive conductor characterized by a macroscopic conductivity σ. Thus, the total current $\mathbf{J}$ at a point $\mathbf{r}$ may be written as:

$$\mathbf{J}(\mathbf{r}) = \mathbf{J}^p(\mathbf{r}) + \sigma(\mathbf{r})\mathbf{E}(\mathbf{r}).$$

Both these contributions to $\mathbf{J}(\mathbf{r})$, in general, affect the distribution of the electric potential as well as the magnetic field. However, it may be shown that if the passive tissue is modelled as a spherically symmetric conductor (which is a model frequently used to analyse the response from the human brain), the volume currents do not contribute to the normal component of magnetic field B_r (which is the component usually measured in a SQUID-based study); it may also be shown that, in a spherically symmetric conductor, the contribution of the volume currents to the tangential components of $\mathbf{B}$ (generally not measured in a SQUID-based study) does not depend on the detailed specification of the conductivity profile $\sigma(\mathbf{r})$ and may be calculated without the knowledge of $\sigma(\mathbf{r})$[15]. This situation also applies to a horizontally layered conductor (which is a model frequently used to analyse the response from the human heart), as this is a limiting case of a sphere as its radius becomes indefinitely large. However, the electric potential V on the surface of a conductor is affected by the conductivity profile $\sigma(\mathbf{r})$ in a nontrivial way making the computation of V lot more complex. If a layer of poorly conducting structure intervenes between the source and the measurement points (for example, skull, ribcage, etc.), the electric potential V is severely attenuated and its distribution on the surface is lot more distorted compared to that of the magnetic field.

For a spherically symmetric conductor and a horizontally layered conductor, the normal component of the magnetic field B_r depends on the primary current $\mathbf{J}^p(\mathbf{r}')$ only

$$B_r(\mathbf{r}) = \frac{\mu_0}{4\pi}\int \mathbf{J}^p(\mathbf{r}') \times \frac{\mathbf{r}-\mathbf{r}'}{|\mathbf{r}-\mathbf{r}'|^3}\cdot \mathbf{e}_r \mathrm{d}^3\mathbf{r}'.$$

From this expression, it is evident that if $\mathbf{J}^p(\mathbf{r}')$ is radially directed, the normal component of the magnetic field on the surface of the conductor will vanish. The measurement of magnetic field using SQUID sensors is therefore sensitive to tangential components of currents only. As both the tangential and radially directed currents contribute to the electric potential V, this fact can be used to discriminate between different types of sources; indeed, by combining the measurements of both the magnetic field $\mathbf{B}$ and the electric potential V, it has been shown that it is possible to provide a more comprehensive account of the underlying process[16]. The tangential components of the source can be reconstructed using the MEG data and the optimum conductivity values can then be estimated by best fitting the EEG data and requiring a precise matching of the tangential components of the source as deduced from MEG. The radial components of the source can then be estimated by using these conductivity values in the analysis of EEG data, allowing one to reconstruct a more comprehensive and trustworthy picture of the source responsible for the generation of MEG/EEG signals.

The problem of estimating the sources responsible for the measured magnetic field distribution is known as the 'inverse problem'; this inverse problem is ill-posed and does not, in general, admit a unique solution[17]. Despite this, it is often possible to impose realistic constraints based on known anatomical and physiological knowledge to recover a physically meaningful solution.

Cryogenic systems and electronic instrumentation

The SQUID sensors have to be cooled to a temperature of 4.2 K for their operation by immersing them in liquid helium. For this, a cryostat using FRP as the material of construction has been selected, as is the norm in such studies, to avoid any magnetic noise associated with eddy currents induced in the body of the cryostat by any resi-

dual magnetic fluctuations in the neighbourhood. The cryostats for MCG and MEG share a common infrastructure. The cryostat for MCG is a flat bottom cryostat with a capacity of about 12 l capable of supporting four SQUID channels. This is being upgraded to a 13 channel system shortly and there are plans to eventually set up a 37 channel cryostat for MCG. We have used the four channel flat bottom cryostat for our initial MEG studies as well to probe signals originating from a limited area of cortex. However, for the simultaneous coverage of the whole head, efforts are underway to set up a concave bottom cryostat with a capacity of 50 l whose bottom surface is shaped like a helmet to accommodate an average adult human head; this cryostat is capable of supporting more than 64 SQUID channels. Each of these liquid helium cryostats has a static hold time exceeding a week, and is supported on a gantry with a nonmagnetic construction. The gantry has a provision to allow a vertical translation of the cryostat up to 400 mm to adjust the height of the cryostat above the floor-level and to allow the axis of the cryostat to be tilted by about 30° depending upon the experimental needs. The bottom flange of the liquid helium cryostat has recesses in which axial gradiometers wound with superconducting wire snugly fit. These recesses serve to reduce the stand-off distance between the warm and cold surfaces of the cryostat to below 10 mm and contribute to an improved signal-to-noise ratio. Each gradiometer consists of two 15 mm diameter loops of superconducting wire separated by a baseline of 50 mm. The superconducting gradiometers serve to inductively couple the external magnetic signals into the SQUID loop via an on-chip integrated input coil, which is tightly coupled to the SQUID. The output of the SQUID is amplified by a battery-operated preamplifier and is processed by flux-locked-loop electronics to provide a linearized SQUID readout signal before it is routed via shielded cables inside the RFSR for analog-to-digital conversion.

The SQUID insert, which goes inside the cryostat, is equipped with radiation baffles in the neck region to avoid radiative heat leak and consequent excessive boil-off of liquid helium. The insert comprises mounting plates at the bottom end to support a set of electrical connectors where the cryostat wiring, encased in a grounded copper foil for the purpose of shielding, is terminated. The gradiometers are inserted through a set of holes drilled in a cylindrical high-density plastic block with a slide-fitting tolerance. The SQUID leads (bias, modulation and heater) are brought out as twisted pairs and soldered onto the designated pins of the electrical connectors fixed on the mounting plate of the insert. The insert is lowered into the cryostat taking due care to ensure that the gradiometers sit snugly inside the 10 mm deep recesses in the bottom flange of the liquid helium cryostat. A photograph of the cryostat installed in the MSR is shown in Figure 6.

The SQUID output is amplified and processed using a flux-locked-loop electronics module based on flux modulation and phase sensitive detection, which serves to linearize the otherwise periodic output of the bare SQUID sensor. The SQUID readout signal, which is proportional to the instantaneous axial gradient $\partial B_z/\partial z$ at the location of the gradiometer, may be further low pass filtered with user desired frequency cut-off which may be set between 30 Hz and 1 kHz depending on the experimental requirements. The filtered SQUID output signal is digitized with a 24 bit resolution using an individual Delta-Sigma ADC in each channel at any user-desired sampling rate up to 200 kHz. The digitized data is transmitted on an optical fibre link capable of supporting data transfer rates up to 75 Mbps to a computer located outside the shielded area. The channel output data as a function of time, together with information on the sensor position coordinates, is stored for subsequent analysis. Data acquisition software, custom designed for this application, allows easy graphical visualization of the data on each channel and incorporates features such as removal of user-identified artefacts and visualization of the data in the frequency domain to investigate the spectral content, etc. The software also enables trigger based epoching and averaging of user-desired number of nominally identical responses such as those evoked in the brain by presenting identical stimuli in succession; the averaging process reveals the evoked response, which is otherwise buried in uncorrelated cortical noise having an order of magnitude higher amplitude.

Figure 6. Photograph of the liquid helium cryostat mounted on the nonmagnetic gantry; the cryostat can be adjusted to be at any desired height from the floor level and can be optionally tilted for the convenience of the subject. The inset shows the SQUID insert with four SQUID channels assembled in place.

Results

The system has been successfully used to measure the extremely low magnetic fields associated with the physiological activities of human heart and brain with a high signal-to-noise ratio. The measurement of the magnetic fields associated with the activity of the heart is MCG, whereas the measurement of the magnetic fields associated with the activity of the brain is MEG.

Magnetocardiography

For the measurement of the MCG signal from the heart, the subject lay supine under the liquid helium cryostat housing the SQUID sensors and the component of the magnetic field normal to the chest surface was measured. Figure 7 shows a representative magnetocardiogram of a 47-year-old male subject recorded in this facility[18]. The SQUID output clearly shows the *P*-wave related to the depolarization of the atria, QRS peak related to the depolarization of the ventricles and the *T*-wave related to the repolarization of the ventricles. The strength of the *R*-peak was over 50 pT and could be measured with a high signal-to-noise ratio since the noise floor was only about 12 fT/√Hz. Such a high signal-to-noise ratio is generally not attainable in a typical ECG measurement. In fact, the MCG signal could also be recorded on the posterior back surface (Figure 8), where it is quite difficult to record the corresponding ECG signal owing to the high electrical resistivity of the air-filled lungs.

It may also be noted that the MCG patterns are morphologically and temporally similar in appearance to the standard ECG as they are the manifestations of the same underlying biological activity. However, the signal-to-noise ratio in MCG is much higher than that in a typical clinical ECG recording because of the inherently high sensitivity offered by the SQUID. In order to comprehensively map the spatial distribution of the cardiac magnetic field on the chest, the measurements have been carried out at a set of points on a 6 × 6 grid fixed on the chest of the subject with reference to the anatomical landmarks[19]. Figure 9 shows the MCG data recorded at 36 different positions on the chest. At each position on the chest, signals corresponding to several cardiac cycles have been averaged to further improve the signal-to-noise ratio. It may be noted that the signal polarity is positive in the upper right half of the figure whereas it is negative in the lower left half. The figure also shows the direction of the

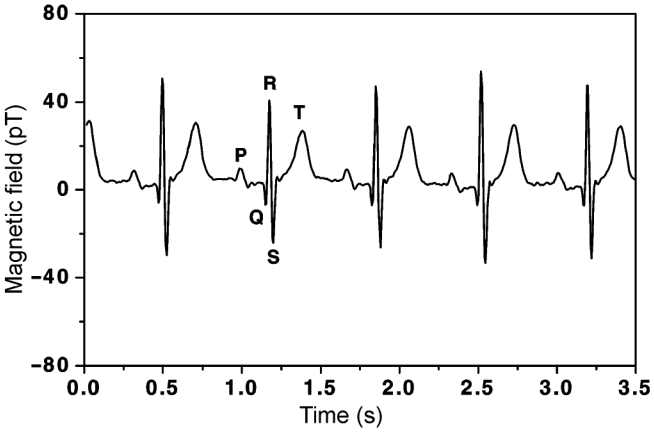

Figure 7. Magnetocardiogram (MCG) of a subject recorded at IGCAR; the *R*-wave peak has an amplitude of about 50 pT while the noise floor is under 12 fT/√Hz. Such a high signal-to-noise ratio is generally not attained in a clinical ECG recording.

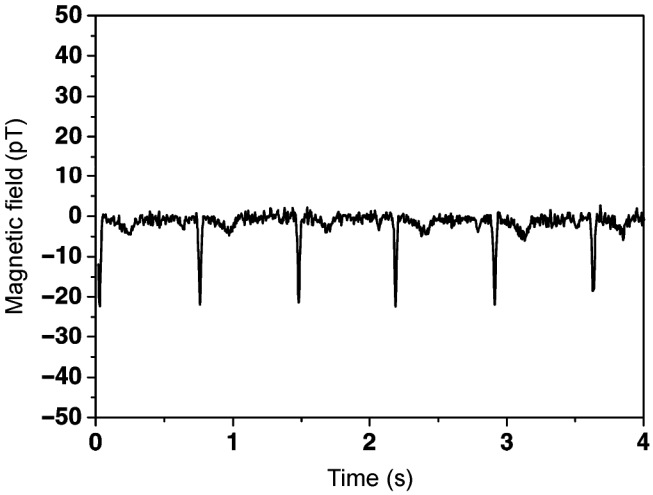

Figure 8. MCG recorded on the posterior back surface of a subject; corresponding ECG often requires an invasive oesophageal lead.

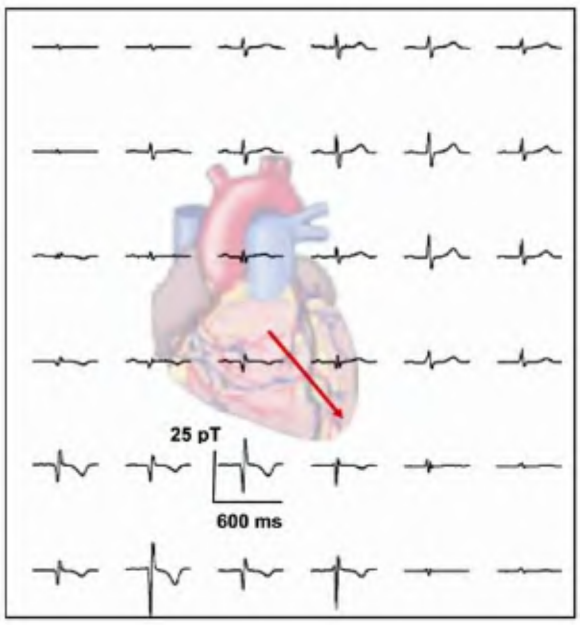

Figure 9. Spatial distribution of cardiac magnetic field sequentially measured at 36 equispaced points on the chest at the nodal points of a square 6 × 6 array with a grid spacing of 4.2 cm; the inferred direction of the equivalent current dipole at the instant when the cardiac cycle is passing through the *R* peak is also shown.

inferred equivalent current dipole when the cardiac cycle is passing through the *R* peak. However, as shown in Figure 10, the iso-field contour maps show the sources to have a more complex configuration than that of a single dipole at any given instant of time.

MCG study of about 40 subjects (both normal subjects and those with cardiac dysfunctions) referred by the DAE Hospital, Kalpakkam has been completed in collaboration with cardiac specialists to assess the potential of this relatively new technique vis-à-vis the more conventional ECG. As an illustration, standard ECG recorded in the hospital and the MCG recorded in the present facility for a 68-year-old male subject with a left bundle branch block (a common cardiac conduction anomaly), is shown in Figure 11. The left bundle branch block leads to a delay in the depolarization of the left ventricle compared to the right ventricle, which manifests as a notched QRS complex in ECG with a duration exceeding 120 ms. It is evident that this delay in the depolarization manifests far more resolved in MCG. This notched QRS complex has been seen in MCG in a number of positions on the chest of the subject[20]. Thus, MCG has the potential to emerge as a powerful diagnostic tool complementing the standard ECG[21].

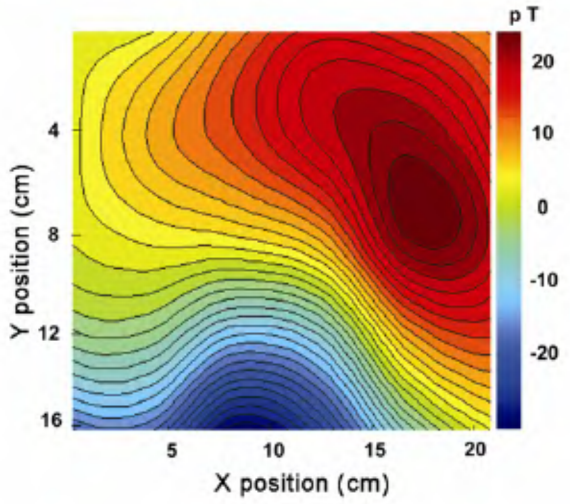

Figure 10. Iso-field contour map constructed at *R* peak using the MCG data. The sources responsible for the recorded activity are seen to be more complex than a single equivalent current dipole.

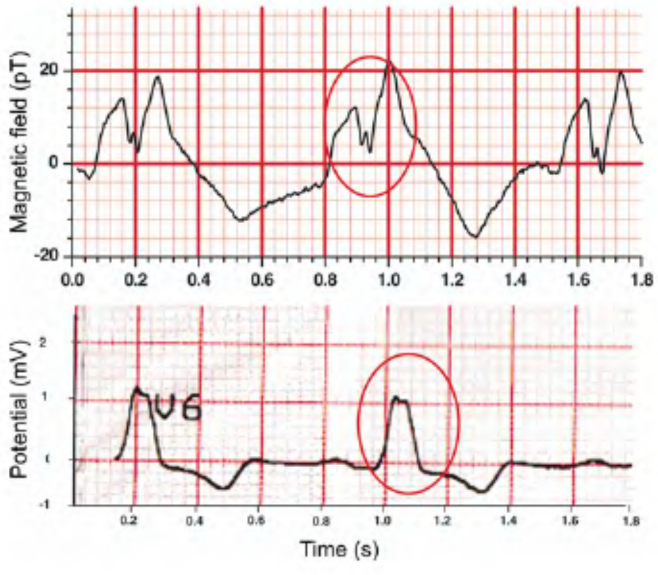

Figure 11. ECG and MCG of a subject with left bundle branch block; MCG data shows clearly resolved notched QRS complex as opposed to the ECG data.

Magnetoencephalography

For the measurement of the MEG signal, the sensor has to be positioned above the scalp of the subject at the desired location. The first MEG signal measured was due to the α rhythm of the brain[22]. For this measurement, the sensor was positioned on the occipital lobe of the brain and the SQUID output was measured sequentially with the subject's eyes open and closed. As shown in Figure 12, the signal in the eyes closed condition was observed to be larger in amplitude and manifested as a peak at about 9 Hz in the Fourier transform as expected; the peak gets suppressed when the eyes are open[18]. This signal is about 50 times weaker in intensity compared to the MCG signal.

The signal associated with eye-saccades and eye-blinks has also been measured by positioning the sensor just above the eyebrow line and signal amplitude of about 2 pT was observed at each eyeblink (Figure 13). It may be noted that such parasitic signals (associated with the eyeblinks, swallowing action, teeth-squeeze, etc.), which are inevitable in a recording session, have to be identified as artefacts during an MEG experiment and eliminated during the data processing. Response of the brain to the presentation of visual/auditory/tactile stimuli tends to be of the order of 100 fT and is generally masked by the

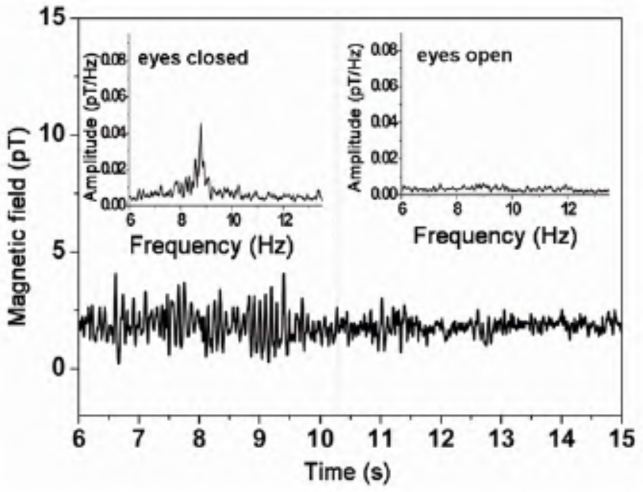

Figure 12. α rhythm monitored from the occipital lobe of the brain; the peak at 9 Hz gets suppressed when the eyes are open (10.5 to 15 s).

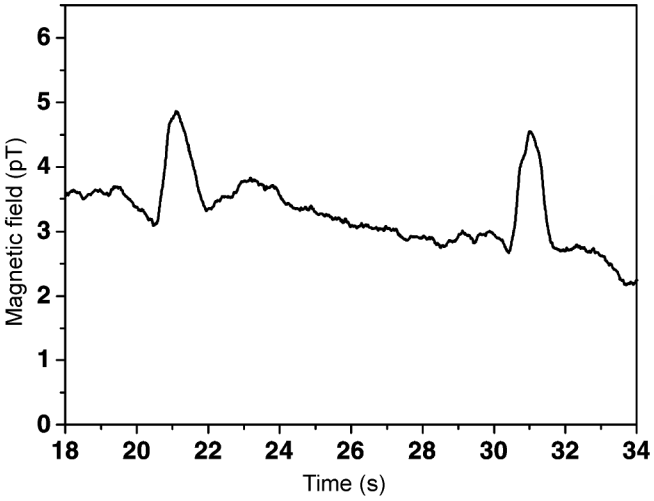

Figure 13. Magnetic signal associated with the eye blink; the subject was instructed to blink his eyes every 10 s.

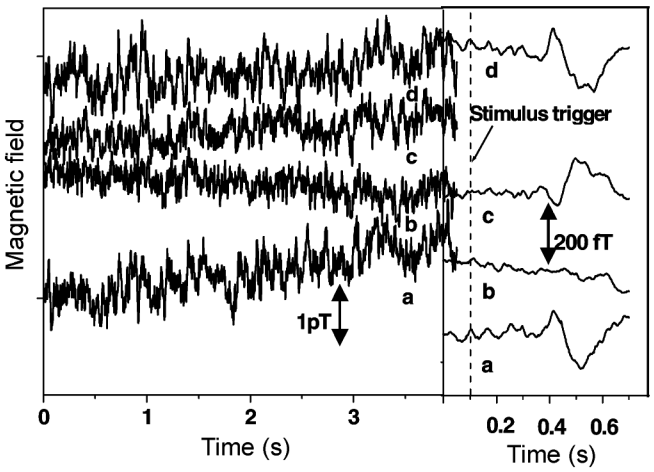

Figure 14. Auditory evoked field measured from the temporal lobe of the brain; the panel on the left shows the raw unaveraged data while the panel on the right shows the averaged data; the response had a latency of about 400 ms from the presentation of the stimulus. a, b, c, d are data from the four channels.

much larger (~2 pT) cortical activity uncorrelated with the presentation of the stimulus; to reveal the evoked response, a large number of responses have to be measured by presenting identical stimuli in quick succession; the recorded nominally identical responses have to be averaged using the stimulus presentation instant as trigger. In this way the response, which is phase-locked to the presentation of the stimulus, stands out whereas the other components of the brain activity which are uncorrelated to the presentation of the stimulus get suppressed. Figure 14 shows the auditory evoked response to the presentation of a 1 kHz pure tone recorded simultaneously at four locations using the four SQUID channel system operational at IGCAR; both the unaveraged and the averaged data have been shown to illustrate the suppression of uncorrelated noise because of the averaging process. As another illustration of the possible experimental methodology, a pure tone with a frequency f (f = 200 Hz, 600 Hz, 1 kHz and 5 kHz) with its amplitude modulated at 23 Hz (with a depth of modulation of about 95%) was presented to a subject using an earphone and the cortical response was monitored over the temporal lobe of the brain using the four channel system sequentially at several positions with a grid spacing of 1 cm along each axis. The 23 Hz modulating waveform was used to provide the necessary reference for averaging a large number of nominally identical data sets. As shown in Figure 15, the process of averaging successfully reveals the underlying cortical response to the auditory stimulation. Such techniques have also been used to study the binaural response from the temporal lobes of both the hemispheres of the brain[23].

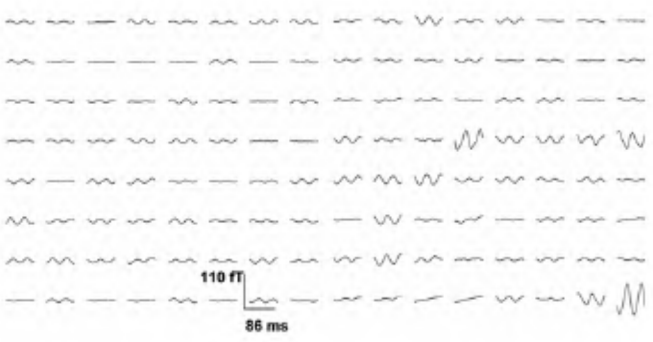

Figure 15. Spatial distribution of the auditory evoked field recorded from the temporal lobe of the brain by presenting a pure tone whose amplitude is modulated at 23 Hz.

Conclusions and future outlook

Facilities have been established at IGCAR for the SQUID-based measurement of biomagnetic fields. These consist of a MSR to house the liquid helium cryostat and SQUID sensors, a RFSR to house the data acquisition system, stimulus presentation system for presentation of specific programmed stimuli in quick succession, etc. Several biomagnetic fields such as those associated with the physiological activities of human heart and brain have been successfully measured. Efforts are on to augment the number of SQUID channels, set up a concave bottom cryostat for whole head coverage in MEG studies and to develop algorithms for source reconstruction from the measured magnetic field distribution. Setting up of multichannel SQUID instrumentation at IGCAR augurs well for studies on how the brain receives, stores and processes the sensory information. There are also possibilities for establishing such SQUID-based systems in a hospital setting in India and using them for clinical applications in areas such as various types of cardiac dysfunctions and focal epilepsy with a view to provide enhanced diagnostic aid eventually leading to better healthcare.

1. Cohen, D., Edelsack, E. A. and Zimmerman, J. E., Magnetocardiograms taken inside a shielded room with a superconducting point-contact magnetometer. *Appl. Phys. Lett.*, 1970, **16**, 278–280.
2. Hamalainen, M., Hari, R., Ilmoniemi, R., Knuutila, J. and Lounasmaa, O. V., Magnetoencephalography – theory, instrumentation, and applications to non-invasive studies of the working human brain. *Rev. Mod. Phys.*, 1993, **65**, 413–487.
3. Del Gratta, C., Pizzella, V., Tecchio, F. and Romani, G. L., MEG – a non-invasive brain imaging method with 1 ms time resolution. *Rep. Prog. Phys.*, 2001, **64**, 1759–1814.
4. Jezzard, E. P., Matthews, P. M. and Smith, M. S. (eds), *Functional MRI: An Introduction to Methods*, Oxford University Press, New York, 2001.
5. Valk, P. E., Bailey, D. L., Townsend, D. E. and Maisey, M. N. (eds), *Positron Emission Tomography: Basic Science and Clinical Practice*, Springer Verlag, London, 2003.
6. Liu, A. K., Belliveau, J. W. and Dale, A. M., Spatiotemporal imaging of human brain activity using functional MRI constrained magnetoencephalography data: Monte Carlo simulations. *Proc. Natl. Acad. Sci. USA*, 1998, **95**, 8945–8950.
7. Im Chang-Hwan, Gururajan, A., Zhang, N., Chen Wei and He Bin, Spatial resolution of high resolution EEG cortical source imaging revealed by localization of retinotopic organization in human primary visual cortex. *J. Neurosci. Meth.*, 2007, **161**, 142–154.
8. Ioannides, A. A., Magnetoencephalography as a research tool in neuroscience: state-of-the-art. *Neuroscientist*, 2006, **12**, 524–543.
9. Williamson, S. J., Romani, G. L., Kaufman, L. and Modena, I., (eds), *Biomagnetism: An Interdisciplinary Approach*, Plenum, New York, 1983.
10. Janawadkar, M. P. *et al.*, SQUIDS – highly sensitive magnetic sensors. *Curr. Sci.*, 1999, **77**, 759–769.
11. Nagendran, R. *et al.*, Development of SQUID based system for non-destructive evaluation. *IEEE Trans. Appl. Supercond.*, 2007, **17**, 3824–3829.
12. Varma, S. K., Kalyanam, J., Murk, L. E. and Srinivas, V., Effect of grain size on deformation-induced martensite formation in 304 and 316 stainless steels during room temperature tensile testing. *J. Mat. Sci. Lett.*, 1994, **13**, 107–111.
13. Radhakrishnan, T. S. *et al.*, Stainless steel bars as reinforcement in concrete: construction of a magnetically transparent building for magnetoencephalography. International Symposium on Advances in Stainless Steels (ISAS-2007), Chennai, India, 9–11 April 2007.
14. Malmivuo, J. and Plonsey, R., *Bioelectromagnetism – Principles and Applications of Bioelectric and Biomagnetic Fields*, Oxford University Press, New York, 1995.
15. Sarvas, J., Basic mathematical and electromagnetic concepts of the biomagnetic inverse problem. *J. Phys. Med. Biol.*, 1987, **32**, 11–22.
16. Huang, M. *et al.*, A novel integrated MEG and EEG analysis method for dipolar sources. *Neuroimage*, 2007, **37**, 731–748.
17. Baillet, S., Mosher, J. C. and Leahy, R. M., Electromagnetic brain mapping. *IEEE Signal Process.*, 2001, **18**, 14–30.
18. Gireesan, K., Parasakthi, C., Sengottuvel, S., Vaidhyanathan, L. S., Baskaran, R., Janawadkar, M. P. and Radhakrishnan, T. S., Magnetocardiogram and magnetoencephalogram using a SQUID based system. *Indian J. Cryogenics*, 2010, **35**, 187–191.
19. Sengottuvel, S. *et al.*, Probing cardiac abnormalities through magnetocardiography. In Proceedings of the 54th Solid State Physics Symposium, 2009, **54**, 453–454.
20. Gireesan, K. *et al.*, Magnetocardiography study of cardiac anomalies, *Advances in Biomagnetism – BIOMAG 2010*, IFBME Proceedings Series, Springer-Verlag, 2010, vol. 28, pp. 431–435.
21. Koch, H., Recent advances in magnetocardiography. *J. Electrocardiol.*, 2004, **37** (*Suppl.*), 117–122.
22. Shaw, J. C., *Brains Alpha Rhythm and the Mind*, Elsevier, Amsterdam, 2003.
23. Kaneko, K., Fujika, N. and Hari, R., Binaural interaction in the human auditory cortex revealed by neuromagnetic frequency tagging: no effect of stimulus intensity. *Hear. Res.*, 2003, **183**, 1–6.

ACKNOWLEDGEMENTS. This work has been carried out as part of a project sponsored by the DST, Government of India with expertise and skills developed over the years under the Department of Atomic Energy. T.S.R., C.P. and S.S. acknowledge the financial support from the DST. The contributions of R. Baskaran, L. S. Vaidhyanathan and R. Nagendran during the execution of this work are also acknowledged.

Received 22 March 2010; accepted 20 April 2010